The Astrophysical Journal Letters, 995:L67 (10pp), 2025 December 20 https://doi.org/10.3847/2041-8213/ae279c

SHELLQs–JWST Perspective on the Intrinsic Mass Relation between Supermassive Black Holes and Their Host Galaxies at $z > 6$

John David Silverman[1,2,3,4], Junyao Li[5], Xuheng Ding[6], Masafusa Onoue[1,7], Michael A. Strauss[8], Yoshiki Matsuoka[9], Takuma Izumi[2,10,11,12], Knud Jahnke[13], Tommaso Treu[14], Marta Volonteri[15], Camryn L. Phillips[8], Irham T. Andika[16,17], Kentaro Aoki[18], Junya Arita[2], Shunsuke Baba[19], Sarah E. I. Bosman[20,21], Anna-Christina Eilers[22], Xiaohui Fan[23], Seiji Fujimoto[24,25], Melanie Habouzit[26], Zoltan Haiman[27,28,29], Masatoshi Imanishi[10], Kohei Inayoshi[30], Kazushi Iwasawa[31,32], Nobunari Kashikawa[2,33], Toshihiro Kawaguchi[34], Chien-Hsiu Lee[35], Alessandro Lupi[36], Tohru Nagao[9,37], Jan-Torge Schindler[38], Malte Schramm[39], Kazuhiro Shimasaku[2,33], Yoshiki Toba[9,40,41], Benny Trakhtenbrot[42,43,44], Hideki Umehata[45,46], Marianne Vestergaard[23,47], Fabian Walter[48], Feige Wang[49], and Jinyi Yang[49]

[1] Kavli Institute for the Physics and Mathematics of the Universe (Kavli IPMU, WPI), UTIAS, Tokyo Institutes for Advanced Study, University of Tokyo, Chiba 277-8583, Japan; silverman@ipmu.jp
[2] Department of Astronomy, Graduate School of Science, The University of Tokyo, 7-3-1 Hongo, Bunkyo, Tokyo 113-0033, Japan
[3] Center for Data-Driven Discovery, Kavli IPMU (WPI), UTIAS, The University of Tokyo, Kashiwa, Chiba 277-8583, Japan
[4] Center for Astrophysical Sciences, Department of Physics & Astronomy, Johns Hopkins University, Baltimore, MD 21218, USA
[5] Department of Astronomy, University of Illinois at Urbana-Champaign, Urbana, IL 61801, USA
[6] School of Physics and Technology, Wuhan University, Wuhan 430072, People's Republic of China
[7] Waseda Institute for Advanced Study (WIAS), Waseda University, 1-21-1, Nishi-Waseda, Shinjuku, Tokyo 169-0051, Japan
[8] Department of Astrophysical Sciences, Princeton University, 4 Ivy Lane, Princeton, NJ 08544, USA
[9] Research Center for Space and Cosmic Evolution, Ehime University, 2-5 Bunkyo-cho, Matsuyama, Ehime 790-8577, Japan
[10] National Astronomical Observatory of Japan, 2-21-1 Osawa, Mitaka, Tokyo 181-8588, Japan
[11] Graduate Institute for Advanced Studies, SOKENDAI, 2-21-1 Osawa, Mitaka, Tokyo 181-8588, Japan
[12] Kagoshima University, Kagoshima 890-0065, Japan
[13] Max Planck Institute for Astronomy, Königstuhl 17, D-69117 Heidelberg, Germany
[14] Department of Physics and Astronomy, University of California Los Angeles, CA 90095, USA
[15] Institut d'Astrophysique de Paris, Sorbonne Université, CNRS, UMR 7095, 98 bis bd Arago, 75014 Paris, France
[16] Technical University of Munich, TUM School of Natural Sciences, Department of Physics, James-Franck-Str. 1, D-85748 Garching, Germany
[17] Max-Planck-Institut für Astrophysik, Karl-Schwarzschild-Str. 1, D-85748 Garching, Germany
[18] Subaru Telescope, National Astronomical Observatory of Japan, 650 North A'ohoku Place, Hilo, HI 96720, USA
[19] Institute of Space and Astronautical Science (ISAS), Japan Aerospace Exploration Agency (JAXA), 3-1-1 Yoshinodai, Chuo-ku, Sagamihara, Kanagawa 252-5210, Japan
[20] Institute for Theoretical Physics, Heidelberg University, Philosophenweg 12, D-69120, Heidelberg, Germany
[21] Max-Planck-Institut für Astronomie, Königstuhl 17, 69117 Heidelberg, Germany
[22] MIT Kavli Institute for Astrophysics and Space Research, Massachusetts Institute of Technology, Cambridge, MA 02139, USA
[23] Steward Observatory, University of Arizona, 933 North Cherry Avenue, Tucson, AZ 85721, USA
[24] Department of Astronomy, The University of Texas at Austin, Austin, TX 78712, USA
[25] David A. Dunlap Department of Astronomy and Astrophysics, University of Toronto, 50 St. George Street, Toronto, ON M5S 3H4, Canada
[26] Department of Astronomy, University of Geneva, Chemin d'Ecogia, CH-1290 Versoix, Switzerland
[27] Institute of Science and Technology Austria (ISTA), Am Campus 1, 3400 Klosterneuburg, Austria
[28] Department of Astronomy, Columbia University, New York, NY 10027, USA
[29] Department of Physics, Columbia University, New York, NY 10027, USA
[30] Kavli Institute for Astronomy and Astrophysics, Peking University, Beijing 100871, People's Republic of China
[31] Institut de Ciències del Cosmos (ICCUB), Universitat de Barcelona (IEEC-UB), Martí i Franquès, 1, 08028 Barcelona, Spain
[32] ICREA, Pg Lluís Companys 23, 08010 Barcelona, Spain
[33] Research Center for the Early Universe, Graduate School of Science, The University of Tokyo, 7-3-1 Hongo, Bunkyo-ku, Tokyo 113-0033, Japan
[34] Graduate School of Science and Engineering, University of Toyama, Gofuku 3190, Toyama 930-8555, Japan
[35] Hobby-Eberly Telescope, McDonald Observatory, UT Austin, 32 Mount Fowlkes, Fort Davis, TX 79734, USA
[36] Como Lake Center for Astrophysics, DiSAT, Universitá degli Studi dell'Insubria, via Valleggio 11, I-22100, Como, Italy
[37] Amanogawa Galaxy Astronomy Research Center, Kagoshima University, 1-21-35 Korimoto, Kagoshima 890-0065, Japan
[38] Hamburger Sternwarte, University of Hamburg, Gojenbergsweg 112, D-21029 Hamburg, Germany
[39] Universität Potsdam, Karl-Liebknecht-Str. 24/25, D-14476 Potsdam, Germany
[40] Department of Physical Sciences, Ritsumeikan University, Kusatsu, Shiga 525-8577, Japan
[41] Academia Sinica Institute of Astronomy and Astrophysics, 11F of Astronomy-Mathematics Building, AS/NTU, No. 1, Section 4, Roosevelt Road, Taipei 10617, Taiwan
[42] School of Physics and Astronomy, Tel Aviv University, Tel Aviv 69978, Israel
[43] Max-Planck-Institut für extraterrestrische Physik, Gießenbachstraße 1, 85748 Garching, Germany
[44] Excellence Cluster ORIGINS, Boltzmannsstraße 2, 85748, Garching, Germany
[45] Institute for Advanced Research, Nagoya University, Furocho, Chikusa, Nagoya 464-8602, Japan
[46] Department of Physics, Graduate School of Science, Nagoya University, Furocho, Chikusa, Nagoya 464-8602, Japan
[47] DARK, The Niels Bohr Institute, University of Copenhagen, Jagtvej 155, 2200 Copenhagen, Denmark
[48] Max-Planck-Institut für Astronomie, Königstuhl 17, D-69117 Heidelberg, Germany
[49] Department of Astronomy, University of Michigan, 1085 South University Avenue, Ann Arbor, MI 48109, USA
Received 2025 July 29; revised 2025 December 2; accepted 2025 December 2; published 2025 December 17

Abstract

The relation between the masses of supermassive black holes (SMBHs) and their host galaxies encodes information on their mode of growth, especially at the earliest epochs. The James Webb Space Telescope (JWST) has opened such investigations by detecting the host galaxies of active galactic nuclei (AGN) and more luminous quasars within the first billion years of the Universe ($z \gtrsim 6$). Here, we evaluate the relation between the mass of SMBHs and the total stellar mass of their host galaxies using a sample of nine quasars at $6.18 \leqslant z \leqslant 6.4$ from the Subaru High-z Exploration of Low-luminosity Quasars survey with NIRCam and NIRSpec observations. We find that the observed location of these quasars in the SMBH–galaxy mass plane ($\log M_{\rm BH}/M_{\odot} \sim 8$–$9$; $\log M_{*}/M_{\odot} \sim 9.5$–$11$) is consistent with a nonevolving intrinsic mass relation with dispersion ($0.80^{+0.23}_{-0.28}$ dex) higher than the local value ($\sim$0.3–0.4 dex) of their more massive descendants. Our analysis is based on a forward model of systematics and includes a consideration of the impact of selection effects and measurement uncertainties with an assumption on the slope of the mass relation. While degeneracies between parameters persist, the best-fit solution has a reasonable AGN fraction (2.3%) of galaxies at $z \sim 6$ with an actively growing UV-unobscured black hole. In particular, models with a substantially higher normalisation in $M_{\rm BH}$ would require an unrealistically low intrinsic dispersion ($\sim$0.22 dex). Consequently, our results predict a large population of AGN at lower black hole masses, as are now just starting to be discovered in focused efforts with JWST.

Unified Astronomy Thesaurus concepts: AGN host galaxies (2017); Scaling relations (2031); Supermassive black holes (1663); High-redshift galaxies (734); Early universe (435)

1. Introduction

The James Webb Space Telescope (JWST; J. Rigby et al. 2023) has opened the landscape of the early Universe and the formation of the first supermassive black holes (SMBHs; K. Inayoshi et al. 2020; M. Volonteri et al. 2021). Deep JWST survey fields routinely find SMBHs with a mass estimated to be $M_{\rm BH} \sim 10^{7-8}\,M_{\odot}$ (e.g., M. Onoue et al. 2023; A. Lupi et al. 2024) and identified as little red dots in many cases (e.g., J. E. Greene et al. 2024; R. Maiolino et al. 2024a; J. Matthee et al. 2024; D. D. Kocevski et al. 2025). In particular, an even lower-mass ($M_{\rm BH} \sim 10^{6}\,M_{\odot}$) black hole may lurk in GN-z11 at $z = 10.6$ (R. Maiolino et al. 2024b). It is imperative to understand their growth history and relation to the more massive black holes at $z \sim 6$, which are observed as luminous quasars.

Astronomers have been making remarkable breakthroughs with JWST in the study of quasars and their massive host galaxies at high redshift. Starlight from quasar host galaxies is now often detected at $z > 6$ (X. Ding et al. 2023; M. A. Stone et al. 2023, 2024; M. Yue et al. 2024; R. Li et al. 2025c; M. Onoue et al. 2025). This is a giant leap from the pre-JWST era, when one could routinely study the stellar properties of hosts only to $z \sim 2$ (K. Jahnke et al. 2004; M. Mechtley et al. 2016; X. Ding et al. 2022a) or in a handful of lensed cases (C. Y. Peng et al. 2006) and mergers (R. Decarli et al. 2019) at higher redshifts.

The Subaru High-z Exploration of Low-luminosity Quasars (SHELLQs) sample (e.g., Y. Matsuoka et al. 2022), constructed from the wide and deep imaging survey with Subaru's Hyper Suprime-Cam (H. Aihara et al. 2018; S. Miyazaki et al. 2018), is playing an important role in bridging the gap between luminous quasars ($M_{\rm UV} < -25$) and the fainter JWST-discovered AGN ($M_{\rm UV} > -22$) at $z \sim 6$. Based on JWST follow-up with NIRCam, the hosts of SHELLQs quasars have high stellar light fractions (up to 70% in F356W; X. Ding et al. 2023, 2025) that enable robust measurements of galaxy sizes (0.6–3.0 kpc) and stellar masses ($M_{*} > 10^{10}\,M_{\odot}$) with a typical precision of 0.3 dex. With NIRSpec, black hole masses are determined to be between $10^{7.8}$ and $10^{9.1}\,M_{\odot}$ based on the broad (FWHM $> 2000\,{\rm km\,s^{-1}}$) Balmer emission lines (X. Ding et al. 2023; Y. Matsuoka et al. 2025; M. Onoue et al. 2025, in preparation). Furthermore, these observations reveal that some quasar hosts exhibit poststarburst signatures (i.e., Balmer absorption lines, Balmer breaks, and lack of spatially extended Hα emission; M. Onoue et al. 2025) suggesting that quasar activity may be tied with quenching in the early Universe.

The relation between black hole mass, $M_{\rm BH}$, and host stellar mass, M_{*}, over cosmic time depends on the connections between the physics of galaxy and black hole growth. Hydrodynamic simulations of galaxy formation vary in their prediction of the relative mass growth of SMBHs and their host galaxies, likely due to differences in black hole seeding, modeling of black hole accretion, and feedback prescriptions for stars, supernova and active galactic nuclei (AGN; M. Habouzit et al. 2022). Observationally, there appears to be little deviation from the local $M_{\rm BH}$–M_{*} relation up to $z \sim 2.5$ (e.g., M. Cisternas et al. 2011; Y. Shen et al. 2015; M. Sun et al. 2015; X. Ding et al. 2020a; J. Li et al. 2021; T. S. Tanaka et al. 2025). However, our current best estimates on the evolution of the mass relation at high redshift depends on accurate accounting of selection biases, measurement uncertainties, and our relatively limited knowledge of the Eddington rate distribution at high redshifts. Even if the systematics are under control, there remains a degeneracy between the evolution rate and the intrinsic scatter, even with the large samples compiled from wide-field ground-based studies up to $z \sim 1$ (J. Li et al. 2021). Pushing observational studies to higher redshift ($z \sim 6$), closer to their formation epoch, offers much promise, since hydrodynamic simulations show larger deviations (M. Habouzit et al. 2022), even though similar biases and selection effects are still present (e.g., A. Schulze & L. Wisotzki 2014; J. Li et al. 2025b) and seen in Atacama Large Millimeter/submillimeter Array studies based on dynamical masses for their hosts (e.g., T. Izumi et al. 2019; J. Li et al. 2022; F. Wang et al. 2024).

The initial results from JWST on AGN and quasars at $z \gtrsim 4$ provide new insights into the mass relation. To date, the majority of observed AGN and quasars at high z (e.g., R. Maiolino et al. 2024a; M. Yue et al. 2024; B. L. Jones et al. 2025; M. A. Marshall et al. 2025; Y. Sun et al. 2025a) with measured stellar masses have black hole masses higher than predicted from the local mass relation (J. Kormendy &

L. C. Ho 2013; A. E. Reines & M. Volonteri 2015; J. E. Greene et al. 2020). This is anticipated when considering the effects of selection biases mentioned above. X. Ding et al. (2023) find that the first two quasars with detected hosts at $z > 6$ lie in a region of the $M_{\rm BH}$–M_* plane, as expected when assuming the local relation and proper treatment of selection effects. For lower-luminosity/mass black holes found by JWST at high z, $M_{\rm BH}/M_*$ has been claimed to lie above the local relation (F. Pacucci et al. 2023; R. Maiolino et al. 2024a). This has been interpreted as a sign of a "heavy seed" formation channel, likely required to explain many of the individual observed cases. However, it has been demonstrated by J. Li et al. (2025b) that selection effects are important even at lower masses when inferring the intrinsic relation, which requires detailed modeling of the expected underlying population of SMBHs and their host galaxies, in the absence of detected systems on or below the local relation. Recently, J. Li et al. (2025a) have demonstrated that such a predicted population of AGN with lower-mass black holes is found in massive galaxies with JWST spectroscopy. S. Geris et al. (2026) further identified a population of low-mass black holes in low-mass galaxies at $3 < z < 7$ located within the scatter of the local relation by stacking deep NIRSpec spectroscopy. Similar cases are being revealed in star-forming main-sequence galaxies at $4 < z < 6$ from the ALPINE/CRISTAL surveys using the JWST NIRSpec integral field unit (IFU; A. L. Faisst et al. 2025, in preparation; W. Ren et al. 2025).

Here, we report on the relation between the mass of SMBHs and their host galaxies at $z > 6$ using a Cycle 1 JWST program that observed 12 low-luminosity quasars from the SHELLQs program (GO 1967; PI: M. Onoue). NIRCam imaging provides the host galaxy detection after careful modeling and subtraction of the quasar emission, while spectroscopy with NIRSpec enables a measure of the black hole mass from the velocity-broadened Balmer emission lines. The details of each of these efforts are fully reported separately (X. Ding et al. 2025; M. Onoue et al. 2025, in preparation). We use the local black hole to host galaxy mass relation of all galaxy types from J. E. Greene et al. (2020) based on dynamically measured black hole masses as a basis for comparison with the high-redshift results. This relation is treated as representative of the overall black hole population in the local Universe. The local relations established for AGN (e.g., A. E. Reines & M. Volonteri 2015) are likely biased toward lower-mass black holes due to an additional AGN duty-cycle-dependent selection bias (A. Schulze & L. Wisotzki 2011; J. Li et al. 2025a) and are therefore not used in our comparison. Throughout this work, we use a Hubble constant of $H_0 = 70$ km s^{-1} Mpc^{-1} and cosmological density parameters $\Omega_m = 0.3$ and $\Omega_\Lambda = 0.7$. We assume a G. Chabrier (2003) stellar initial mass function to infer the host galaxy masses.

2. Data and Measurements

2.1. Sample Selection

Twelve quasars were selected from an early sample of 50 low-to-moderate-luminosity ($M_{1450} > -26$ mag) SHELLQs quasars discovered by Subaru's Hyper Suprime-Cam (HSC; H. Aihara et al. 2018) over 650 deg^2, spectroscopically confirmed from ground-based observations (mainly by their Lyα emission; Y. Matsuoka et al. 2016, 2018b, 2018a), and included in the luminosity function reported in Y. Matsuoka et al. (2018c). The properties of these quasars are listed in Table 1 of X. Ding et al. (2025) and shown in Figure 1 along with the selection completeness, ranging from 42% to 86%. Their redshifts are between 6.18 and 6.40, on the high end of the parent SHELLQs sample (Y. Matsuoka et al. 2022). These quasars were chosen to have faint absolute magnitudes ($-24 < M_{1450} < -21$) to minimize the challenge of detecting the host galaxy under the emission from an unresolved bright point source. For this study, we remove the three faintest quasars with $M_{1450} \gtrsim -22$ (HSC J0911+0152, HSC J1146 −0005, and HSC J1512+4422), since they were added to the JWST program with a different selection from the brighter targets, i.e., not from the sample of Y. Matsuoka et al. (2018c). The final sample has nine quasars with $-24 < M_{1450} < -23$. For each, we have made an assessment of the completeness (bottom right panel of Figure 1), with respect to being selected from HSC photometry as a high-z quasar by a Bayesian criterion, using a large mock sample with Sloan Digital Sky Survey (SDSS)–like quasar spectra, a modified Lyα equivalent-width distribution to match HSC quasars, and intergalactic medium absorption as fully detailed in Section 3.4 of Y. Matsuoka et al. (2018c).

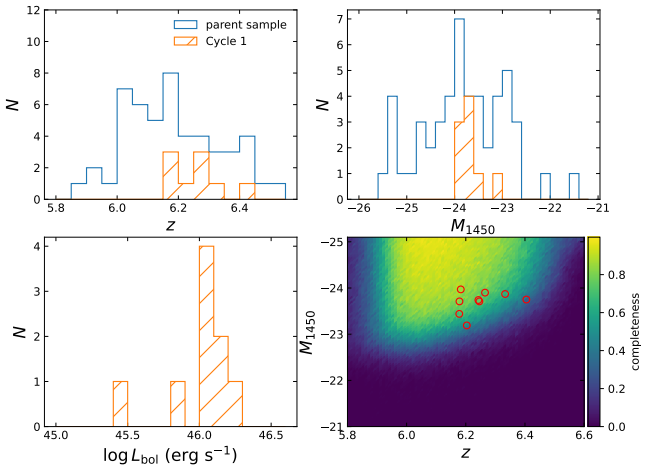

Figure 1. Properties of the Cycle 1 sample as drawn from SHELLQs (Y. Matsuoka et al. 2018c): redshift, absolute UV magnitude, bolometric luminosity, and selection completeness as a function of absolute magnitude and redshift.

2.2. Stellar and Black Hole Masses with JWST

NIRCam and NIRSpec observations of these nine SHELLQs quasars were taken in Cycle 1 as fully described by X. Ding et al. (2023, 2025) and M. Onoue et al. (2025). The primary aim was to measure the stellar mass of the host galaxy using NIRCam and the mass of the black hole responsible for the quasar emission with NIRSpec.

NIRCam images of each quasar are taken in the F356W ($\lambda_{\rm rest} \sim 0.488\,\mu$m) and F150W ($\lambda_{\rm rest} \sim 0.206\,\mu$m) filters. The pixel scales are 0.″0315 (F356W) and 0.″0153 (F150W). For each image, the emission is fit using Galight (X. Ding et al. 2021) with a two-component model, representing the quasar and its host galaxy. The quasar component is based on a characterization of the point-spread function (PSF; X. Ding et al. 2025), while the host galaxy is represented as a Sérsic function. Briefly, the host galaxies are detected in the F356W filter for all nine quasars based on satisfying three conditions: a host-to-total flux ratio greater than 3% (based on extensive

simulations of quasar+host decomposition), signal-to-noise of the host ($\geqslant$2), and improvement in the Bayesian information criterion (ΔBIC $>$ 50) when including the host component in the modeling (X. Ding et al. 2025). The host-to-total ratios vary from $\sim$4% to $\sim$69%. Six of the nine quasars are also detected in the F150W filter and are significantly fainter with lower signal-to-noise ratios. Uncertainties on the best-fit parameters are assessed by varying the method and stars used to construct the PSF model.

We infer the host stellar mass by fitting the available photometry with SED models through the software package GSF (T. Morishita et al. 2019), which results in the range of $10^{9.5-11}\,M_{\odot}$. Eight of the nine quasars hosts have photometry in two filters (F356W and F150W) that bracket the Balmer break at their redshifts. For J2236+0032, the host is observed with eight filters, thus providing an accurate assessment of the underlying stellar population (M. Onoue et al. 2025) that lends weight to the robustness of the results for those with only two filters. Upper limits are used for those with nondetections in F150W. In addition to a chosen G. Chabrier (2003) initial mass function, the spectral energy distributions are mainly dependent on stellar age, metallicity (Z), and dust attenuation (A_V). Typical stellar mass errors are 0.35 dex, encompassing the uncertainties in these parameters (age, Z, and A_V), and are each reflective of errors in the host photometry resulting from varying the method of 2D decomposition as mentioned above. The three quasars with single-band detections in F356W are used here with larger uncertainties ($\sim$0.4–0.5 dex) on their stellar masses as reported in X. Ding et al. (2025), who provide a full description of the assumptions on the parameters and their uncertainties.

NIRSpec observations with a fixed slit and G395M grating ($R \approx 1000$; 2.87 μm $< \lambda_{\rm obs} <$ 5.27 μm) provide a wealth of spectral information for understanding the physical nature of quasar emission and, if detected, the underlying host galaxy. We model the continuum and emission lines to measure the velocity widths of the broad Balmer emission lines, Hα and Hβ. Here, we use the single-epoch virial method to determine black hole masses based on Hβ (M. Vestergaard & B. M. Peterson 2006), the same method that is used for local scaling relations. The resulting black hole masses are found to be in the range of $M_{\rm BH} = 10^{8-9}\,M_{\odot}$ for all objects in the sample[50] except one at $M_{\rm BH} = 10^{7.2}\,M_{\odot}$, as shown in Figure 2. The uncertainties are at the level of 0.4 dex (Y. Shen et al. 2024), which is taken into consideration in our analysis described below.

3. Method to Account for Selection Biases and Measurement Uncertainties

There are numerous works (e.g., T. R. Lauer et al. 2007; T. Treu et al. 2007; A. Schulze & L. Wisotzki 2011, 2014) highlighting the potential for strong biases in SMBH–host galaxy mass relations when using AGN in flux-limited samples, particularly those extending to high redshifts. Here, we follow the recent procedure described by J. Li et al. (2025b) to infer the underlying $M_{\rm BH}$–M_* relation from the observed data points. Recently, studies have begun to apply such corrections for selection effects when evaluating the intrinsic mass relation (J. Li et al. 2021, 2022; F. Pacucci et al. 2023; Y. Sun et al. 2025b; T. S. Tanaka et al. 2025).

We briefly describe the procedure for determining the likelihood distributions on model parameters descriptive of the intrinsic mass relation at high redshift while referring the

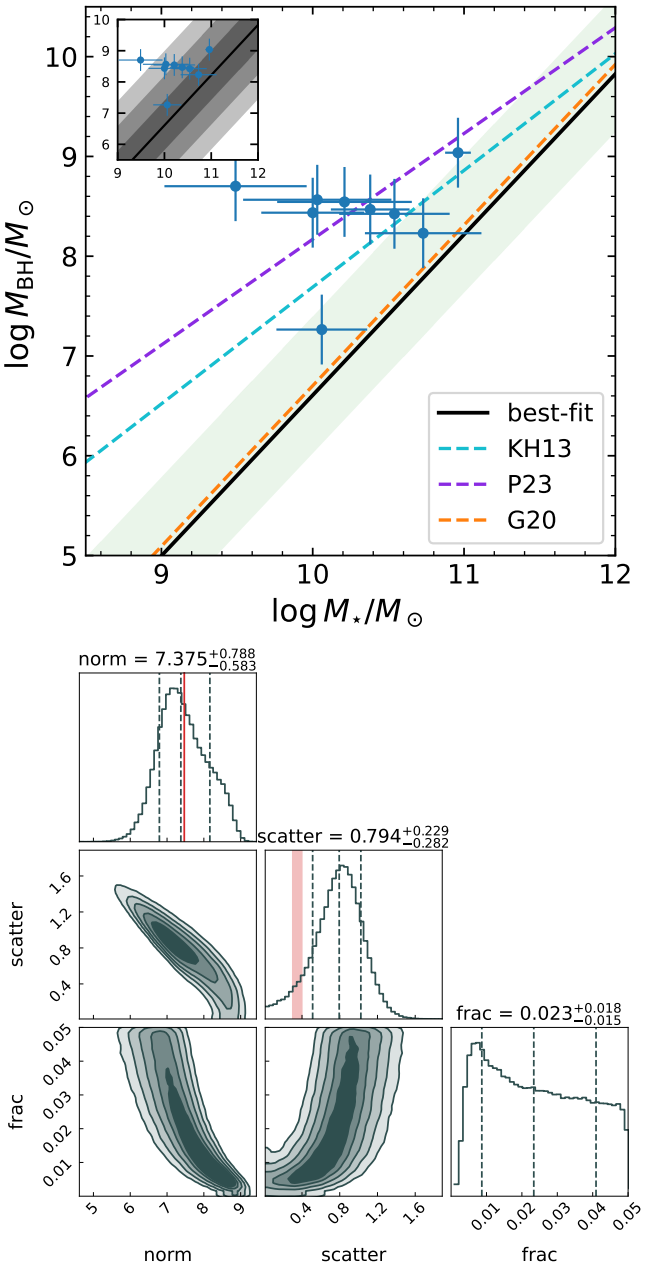

Figure 2. Top: black hole mass ($M_{\rm BH}$) versus stellar mass (M_*) of the host galaxy for the nine SHELLQs quasars. The best-fit relation (black line) and uncertainty (1σ; shaded area) are indicated and incorporate selection biases and measurement uncertainties. Local relations of J. E. Greene et al. 2020 (G20) and J. Kormendy & L. C. Ho 2013 (KH13) are also indicated, along with the high-z assessment of F. Pacucci et al. 2023 (P23) using JWST AGN in CEERS (D. D. Kocevski et al. 2025) and JADES (R. Maiolino et al. 2024a). The inset plot displays the location of the observed quasar sample with respect to our best-fit relation with shaded areas marking the intrinsic scatter (1σ–3σ). Bottom: best-fit inference on model parameters (normalization, scatter of the linear mass relation, and AGN fraction) with the slope fixed to 1.61. The normalization of the G20 relation is indicated by the vertical red line in the top panel, while the local intrinsic dispersion of massive local galaxies (K. Gültekin et al. 2009; J. Kormendy & L. C. Ho 2013; J. E. Greene et al. 2020; V. N. Bennert et al. 2021) is shown by the red vertical band in the top middle panel.

[50] For one quasar (J0217–0208), R. Marques-Chaves et al. (2025) claim that the broad lines are due to an outflow rather than emission from the AGN broad-line region. Even so, we include this object in our quasar sample.

reader to J. Li et al. (2025b) for the details. A forward model of the intrinsic linear $M_{\rm BH}$–M_* relation in log space is implemented with constraints from the observed values of $M_{\rm BH}$, M_*, and their number counts within the survey area. Our modeling requires key distribution functions describing the underlying true galaxy and black hole populations.

Explicitly, a functional form of the conditional probability distribution for detecting a quasar is constructed as a function of the observed stellar mass, black hole mass (assuming Gaussian uncertainties), bolometric luminosity, emission-line width, active unobscured AGN fraction, and redshift (see Equation (4) in J. Li et al. 2025b). First, we start with an analytic form of the stellar mass function of galaxies as a function of redshift from M. Shuntov et al. (2025). SMBHs are connected to galaxies through the $M_{\rm BH}$–M_* mass relation, which is described by its slope (β), normalization (α), and intrinsic scatter (σ). We parameterize the linear mass relation following J. E. Greene et al. (2020) as

$$\log M_{\rm BH}/M_\odot = \alpha + \beta \log (M_*/M_0) + \sigma, \quad (1)$$

where $M_0 = 3 \times 10^{10}\ M_\odot$ and σ is the intrinsic Gaussian scatter, i.e., not including measurement errors. The Eddington rate distribution function (ERDF) provides the means to assign a likelihood distribution to the bolometric quasar luminosity, which then determines whether an individual quasar is luminous enough to be included in the SHELLQs sample. We implement the lognormal ERDF at $z \sim 6$ provided by J. Wu et al. (2022), which peaks at $\log \lambda_{\rm Edd} \sim -1.0$ with a scatter of $\sim$0.4. The unobscured broad-line AGN fraction indicates the population of galaxies with actively accreting SMBHs following the assumed ERDF and selection as *UV-unobscured* quasars by SHELLQs. To be conservative, we constrained this fraction ($p_{\rm active}$) to be less than 5% assuming a flat prior, motivated by recent clustering-based estimates of the duty cycle of SHELLQs quasars ($\sim$1.9%; J. Arita et al. 2023). Adopting higher values (e.g., up to $\sim$20%) based on recent studies of JWST optically selected broad-line AGN (Y. Harikane et al. 2023; R. Maiolino et al. 2024b; J. Li et al. 2025b) would shift the recovered intrinsic mass relation (Section 4) further downward in the $M_{\rm BH}$–M_* plane to avoid overproducing detectable quasars. Nevertheless, this does not affect our conclusion that a large population of low-mass black holes is likely missed (Section 4).

The selection function is mainly based on the quasar limiting luminosity, above which a photometrically selected quasar would be targeted for spectroscopic follow-up. A range in luminosity ($46 < \log L_{\rm bol}/({\rm erg\ s^{-1}}) < 46.2$) is imposed that is representative of the Cycle 1 sample (Figure 1). Bolometric luminosities are computed using a correction factor from G. T. Richards et al. (2006) with $L_{\rm bol} = 9.26\, L_{5100}$. There is a further restriction on the broad-line widths to be greater than 2000 km s^{-1}. Equations (5)–(7) in J. Li et al. (2025b) give the formulation for calculating the selection function, the bivariate distribution function of observed masses with measurement uncertainties, and the derivation of the observed mass relation, expected from the modeling given the selection function.

The modeling procedure presented by J. Li et al. (2025b) requires a comparison of the model-predicted number counts of detectable quasars, within the observed stellar mass ranges, with the actual detected numbers (i.e., ensuring the proper normalization) to determine the best-fit model assuming Poisson likelihood. We first apply a kernel density estimate to our sparse stellar mass distribution (corrected using the incompleteness in Figure 1) to estimate the number of quasars in the following stellar mass bins: $\log M_*/M_\odot < 9.5$, $9.5 < \log M_*/M_\odot < 10.0$, $10.0 < \log M_*/M_\odot < 10.5$, $10.5 < \log M_*/M_\odot < 11.0$, and $\log M_*/M_\odot > 11.0$, yielding 0.7, 2.7, 3.4, 3.9, and 1.1 sources, respectively. Since the Cycle 1 sample represents only a subset of quasars detected by SHELLQs, we further use the bolometric luminosity function of SHELLQs quasars, converted from the UV luminosity function in Y. Matsuoka et al. (2018c) assuming $L_{\rm bol} = 3.81 \times L_{1450}$ (G. T. Richards et al. 2006), to estimate the total number of quasars at $\log L_{\rm bol} \sim 46.1$ (units of erg s^{-1}). This results in a correction factor of $\sim$1.4 (i.e., ratio of true quasars to those observed by JWST). In our fitting procedure, we assume that these missing objects follow the same $M_{\rm BH}$–M_* relation as those in the Cycle 1 sample. Lastly, we refrain from merging samples from the literature with widely different selection functions, which are a challenge to model simultaneously.

4. Results

The top panel of Figure 2 shows the location of the nine SHELLQs quasars in the $M_{\rm BH}$–M_* plane. Their masses mostly span an interval of $8 < \log M_{\rm BH}/M_\odot < 9$ and $9.5 < \log M_*/M_\odot < 11$. Similar to most quasar-selected samples at high redshift (e.g., M. Yue et al. 2024), the observed values fall above the local mass relations; i.e., their black hole masses are higher, given the stellar masses of their host galaxies. Their location is similar to where the two SHELLQs quasars were first reported in X. Ding et al. (2023) as observed by JWST. However, the observed sample is affected by selection biases and is thus not representative of the intrinsic distribution without additional inference. As demonstrated below, a proper modeling of the selection effects and measurement uncertainties provides insight into the underlying intrinsic population.

Our aim here is to use the observed sample and our forward-modeling procedure (J. Li et al. 2022, 2025b) with selection biases and measurement uncertainties incorporated to infer the underlying intrinsic mass relation between SMBHs and their hosts. As done in J. Li et al. (2025a), we sample the conditional probability distributions, described in Section 3, using emcee (D. Foreman-Mackey et al. 2013) to determine the most likely $M_{\rm BH}$–M_* relation, primarily the normalization (α) and scatter (σ) from Equation (1). Given the limited size and dynamic range in black hole mass of the SHELLQs–JWST sample, we fixed the slope (β) to 1.61—the value of the local relation reported in J. E. Greene et al. (2020)—since the slope is unconstrained in our fitting and tends to hit the upper limit when left free.

In the bottom panel of Figure 2, the results are presented from the forward modeling of the $M_{\rm BH}$–M_* relation. The likelihood distributions of each parameter are reported from left to right along the bottom axis: (1) normalization (α) of the linear relation, (2) dispersion (σ) in the mass ratio, and (3) fraction of galaxies ($p_{\rm active}$) hosting UV-unobscured broad-line AGN.

Based on the fixed slope, the best-fit intrinsic $M_{\rm BH}$–M_* relation at $z > 6$ is shown by the black line and shaded area in Figure 2 (top panel), which has a normalization (α) of $7.38^{+0.79}_{-0.58}$ at $M_{*,0} = 3 \times 10^{10}\, M_\odot$. This is consistent with the

local relation of J. E. Greene et al. (2020) based on all galaxy types[51] while falling below the $M_{\rm BH}$–$M_{\rm bulge}$ relation of massive bulge-dominated galaxies from J. Kormendy & L. C. Ho (2013). This result is inconsistent with the intrinsically overmassive relation of F. Pacucci et al. (2023), shown by the dashed purple line, which is based on less massive galaxies having $7.5 \lesssim \log M_*/M_\odot \lesssim 10$ and $6.5 \lesssim \log M_{\rm BH}/M_\odot \lesssim 8$. We note that adopting a flatter slope in the fitting, such as the value from the J. Kormendy & L. C. Ho (2013) relation ($\beta = 1.17$), does not affect our main conclusion, although it results in a significantly poorer fit.

Our model constrains the intrinsic scatter of the $M_{\rm BH}$–M_* relation to be $0.80^{+0.23}_{-0.28}$ dex. If we increase the uncertainties to 0.45 dex on average to our black hole mass measurements, the best-fit scatter increases to 0.85 dex. We compare the dispersion at high z with that of massive ($\log M_* \gtrsim 11$) galaxies at low z, which are likely the descendants of the high-z quasars. The scatter, now determined at $z > 6$, is significantly higher than local massive galaxies (0.3–0.4 dex; K. Gültekin et al. 2009; J. Kormendy & L. C. Ho 2013; J. E. Greene et al. 2020; V. N. Bennert et al. 2021) and low-redshift AGN, considering spheroid (V. N. Bennert et al. 2021) or total stellar (M. C. Bentz & E. Manne-Nicholas 2018; A. E. Reines & M. Volonteri 2015) masses. We note that J. E. Greene et al. (2020) report a higher intrinsic scatter of 0.65 ± 0.05 when including lower-mass galaxies down to $\sim 10^{10}$ $M_\odot$, which warrants further investigation on the appropriate local scatter for comparison to high-z estimates, which is beyond the scope of this work.

As a consistency check on the model of our best-fit mass relation for an assumed ERDF, we successfully reproduce the distribution of the observed sample in both the $M_{\rm BH}$–M_* and $M_{\rm BH}$–Eddington ratio planes (Figures 3(a) and (b)). Our model constraint on the number counts of UV-unobscured quasars results in agreement with the luminosity function of Y. Matsuoka et al. (2018c) as shown in Figure 3(c). This is then reflected in the best-fit unobscured active fraction ($p_{\rm active} = 2.3^{+1.8}_{-1.5}\%$) of UV-unobscured quasars, which generally agrees with the duty cycle measured through clustering analysis of quasars at $z > 6$ (J. Arita et al. 2023; A.-C. Eilers et al. 2024).

As a result, the fact that the observed SHELLQs quasars lie above the local relation in the $M_{\rm BH}$–M_* plane is due to the dispersion in the intrinsic mass relation and the effects of selection and measurement uncertainties. While the observed quasars do have such high mass ratios individually, selection makes them biased tracers of the underlying global population that has lower mass ratios.

However, there are considerable degeneracies between the parameters shown by the confidence intervals in the bottom panels of Figure 2. For instance, a higher normalization results in both a lower scatter (middle left panel) and lower AGN fraction (bottom left panel). Due to the limited sample size, the AGN fraction is poorly constrained within our chosen bounds (bottom right panel). While a peak is apparent in the AGN fraction at low values ($\lesssim$0.01), such a low value is unlikely since the scatter would be forced to be very low ($\sim$0.2).

To further illustrate these effects, we show a similar set of panels in Figure 4 for the case that requires a higher normalization (i.e., forcing a high black hole mass solution) by simply setting a prior on the lower bound of α to match the local value of massive ellipticals from J. Kormendy & L. C. Ho (2013). For this experiment, the slope (β) is fixed to that of the J. Kormendy & L. C. Ho (2013) relation (1.17), which is close to the best-fit value when the slope range is

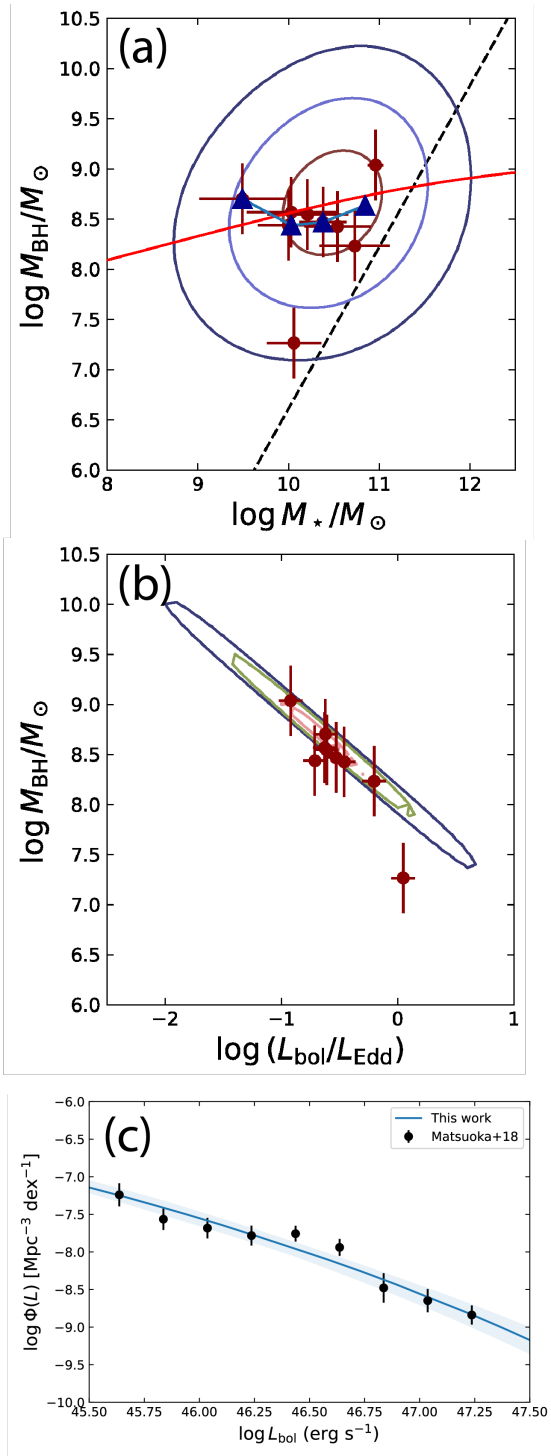

Figure 3. Model comparison to the observed sample. (a) Bivariate mass distribution (1σ–3σ contours). The red curve and blue triangles show the mean mass relation of the observed model distribution and the observed data for the nine SHELLQs quasars, respectively. The recovered intrinsic mass relation is shown by the dashed line. (b) Observed distribution in the $M_{\rm BH}$ versus Eddington ratio plane with the model prediction (1σ–3σ contours). (c) Best-fit model luminosity function compared to that from Y. Matsuoka et al. (2018c).

[51] We consider the J. E. Greene et al. (2020) relation for all galaxy types appropriate for comparison since many of the hosts at $z > 6$ resemble disklike galaxies (X. Ding et al. 2025).

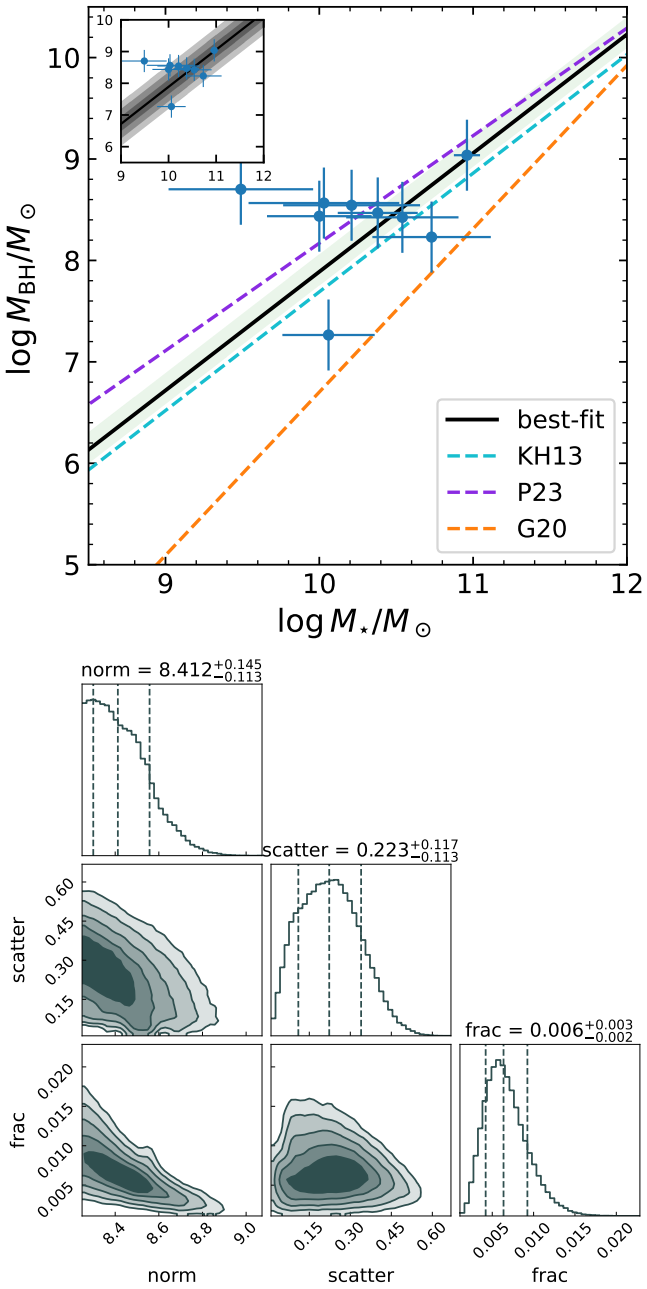

Figure 4. Same as Figure 2 but with the intrinsic mass relation forced to be larger than the J. Kormendy & L. C. Ho (2013) relation (i.e., the overmassive case) and the slope fixed to 1.17. As shown, this case demands a mass relation with very little dispersion (0.22, even less than the local relation) and a very low AGN fraction (0.6%); therefore, this solution is not preferred.

limited to the values spanned by various local relations (∼0.98–1.61; J. Kormendy & L. C. Ho 2013; J. E. Greene et al. 2020; X. Ding et al. 2022b). The best-fit result (top panel of Figure 4) is consistent with our observed quasars and closer to the best-fit relation of F. Pacucci et al. (2023). However, this comes with two consequences: the scatter ($\sigma = 0.22^{+0.12}_{-0.11}$ dex) and AGN fraction ($p_{\rm active} = 0.6^{+0.3}_{-0.2}\%$) are significantly lower than the above model shown in Figure 2, in order to avoid overproducing large numbers of detectable quasars that are not observed. Intuitively, this trend can be understood as follows. With a higher normalization that falls closer to the observed data, the intrinsic scatter will be lowered, since the differences

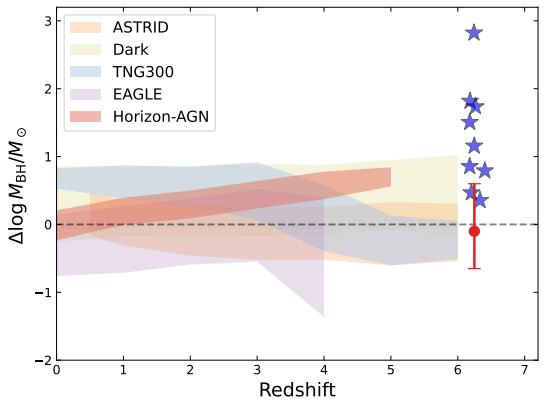

Figure 5. Best-fit value and 1σ confidence interval of the intrinsic mass ratio (red data point) relative to the local J. E. Greene et al. (2020) relation for the ensemble of nine SHELLQs–JWST quasars. The observed mass ratios for the individual quasars are shown as blue stars. The results from five cosmological hydrodynamic simulations and semianalytic models at $\log M_*/M_\odot \sim 10.5$ are indicated (M. Habouzit et al. 2021; S. Dattathri et al. 2025) between the 16th and 84th percentiles.

between the two are effectively reduced. As mentioned above, this covariance between the scatter and normalization is clearly seen in the bottom panels of Figure 2. Furthermore, this effect is amplified by the fact that some of the scatter in the data is the result of measurement uncertainties in $M_{\rm BH}$ and M_*.

In this scenario with a higher normalization, a low intrinsic scatter of 0.22 dex is unlikely since this value is lower than measured locally (∼0.3–0.4 dex). A higher intrinsic dispersion is expected at higher redshifts simply from cosmic averaging (i.e., the central limit theorem) in merger scenarios (K. Jahnke & A. V. Macciò 2011). With the likelihood of a higher intrinsic dispersion and probably an actual AGN fraction above 1% (e.g., J. Arita et al. 2023), we conclude that the intrinsic mass relation at $z \sim 6$ is unlikely to be highly elevated from the local relation.

4.1. Comparison to Simulations

The high-redshift Universe offers an early environment to disentangle the physical processes responsible for the growth of SMBHs and their host galaxies. The observational data at $z > 6$ may be used to discriminate between the importance of various input physics implemented in cosmological simulations, including the seeding of black holes, their subsequent growth, and feedback processes for supernovae and AGN. With this in mind, we compare our results in Figure 5 with four cosmological simulations of galaxy and black hole growth, namely, ASTRID (Y. Ni et al. 2022), TNG300, (A. Pillepich et al. 2018), Horizon-AGN (M. Volonteri et al. 2016), and EAGLE (J. Schaye et al. 2015), as well as the Dark Sage semianalytic model (A. R. H. Stevens et al. 2016, 2018). Since these simulations do not have a sufficiently large volume to produce black holes with masses comparable to those powering the most massive high-redshift quasars, our comparison is necessarily based on an extrapolation from lower-mass black holes.

The mass ratios vary by 1 to 2 dex across the different simulations and semianalytic models, highlighting the lack of consensus on whether black holes are, on average, more or less massive at high redshift compared to low redshift. In other words, the offsets indicate whether black hole growth proceeds more rapidly or more slowly than the assembly of their host

galaxies at early cosmic times. Comparison with observations of high-redshift quasars can therefore diagnose a combination of physical processes such as black hole initial mass and growth and feedback processes from supernovae and AGN.

Simulations such as ASTRID show an $M_{\rm BH}$–M_* relation that remains relatively unchanged in both normalization and shape with redshift. Black holes and their host galaxies evolve in a similar manner across different redshifts. In contrast, models like Horizon-AGN exhibit smaller mass offsets at lower redshift, which can be attributed to galaxies growing more rapidly than their central black holes at later epochs. For TNG300, the growth of black holes in low-mass galaxies is more strongly suppressed at high redshift compared to low redshift due to the modeling of supernova feedback. This results in an increase in the mass ratios as redshift decreases.

In Figure 5, we compare the black-hole-to-stellar-mass ratios of our individual quasars (observed; blue stars) and the intrinsic mass ratio (red circle and error bar) to the simulations at $\log M_*/M_\odot \sim 10.5$ (including inactive black holes) and up to $z \sim 6$ (M. Habouzit et al. 2021; S. Dattathri et al. 2025). The 16th–84th percentile ranges indicate the intrinsic scatter in the mass offset for each model. As shown, the variations in the mass ratio between the models are generally similar to the observed 1σ confidence interval on our best inference on the intrinsic mass ratio at $z > 6$. It is worth highlighting once again how closely our measurement matches that of the local relation of J. E. Greene et al. (2020). As evident, a larger observed sample at $z \gtrsim 6$ is needed along with the inclusion of lower-redshift samples (e.g., X. Ding et al. 2020b, 2022b; T. S. Tanaka et al. 2025) to place substantive constraints on current simulations and models.

5. Summary

A determination of the evolution in the intrinsic mass relation between SMBHs and their host galaxies is needed to understand the coupling and mutual influence on their growth. While much effort has been achieved at lower redshifts ($z \lesssim 2$), the Universe at $z > 6$ represents early phases of SMBH growth, likely more sensitive to the initial conditions (i.e., seeding and feedback mechanisms).

Toward this goal, we use a sample of nine quasars at $z > 6$ from the SHELLQs survey, observed with JWST, in conjunction with an established forward-modeling approach to account for selection biases and measurement uncertainties to assess the intrinsic mass relation between SMBHs and their host galaxies. Black hole masses are based on NIRSpec observations of the broad Balmer lines (M. Onoue et al. 2025, in preparation), while the stellar masses of their host galaxies are measured from the 2D decomposition of NIRCam images (X. Ding et al. 2023, 2025). We assume that the observed location of these nine quasars in the $M_{\rm BH}$–M_* plane is representative of the larger sample of SHELLQs quasars from Y. Matsuoka et al. (2018c). Our forward modeling of the relation between SMBHs and their hosts depends on knowledge of the stellar mass function of galaxies and the Eddington rate distribution. Output parameters are the normalization (α) and scatter (σ) of the intrinsic mass relation along with the AGN fraction ($p_{\rm active}$). The slope (β) of the mass relation is fixed to the local value of 1.61 (J. E. Greene et al. 2020) due to the small sample over a limited range in mass.

Based on our best understanding of the data and selection effects, we find that the intrinsic mass relation between SMBHs and their stellar mass is unlikely to be elevated much above the local mass relation. Rather, observational selection effects and measurement uncertainties result in the observed offsets seen in the $M_{\rm BH}$–M_* plane. Based on a fixed slope in the mass relation, the intrinsic relation at $z > 6$ is consistent with the local relation of J. E. Greene et al. (2020), which may indicate a scenario where SMBHs and the total stellar mass of their host galaxies grow in tandem.

Interestingly, the dispersion ($0.80^{+0.23}_{-0.28}$ dex) in the mass relation at $z > 6$ is higher than the local value ($\sim$0.3–0.4 dex) of their likely more massive descendants. Evolution in the dispersion has not been seen in studies at lower redshifts, particularly based on a large SDSS quasar sample at $z < 1$ with Subaru's Hyper Suprime-Cam ($\sigma = 0.25^{+0.03}_{-0.04}$ dex; J. Li et al. 2021) and AGN at $1 \lesssim z < \lesssim 2$ with JWST ($\sigma = 0.38^{+0.12}_{-0.09}$ dex; T. S. Tanaka et al. 2025). This new result may support a noncausal connection between galaxies and their SMBHs, i.e., a natural outcome of cosmic averaging due to mergers (K. Jahnke & A. V. Macciò 2011). However, there is uncertainty on the level of scatter (along with the normalization) due a degeneracy with the active fraction, which requires better constraints. Furthermore, we recognize that the dispersion in mass relations is dependent on galaxy type; thus, these conclusions depend on the choice of the local samples employed. A more focused analysis based on these results and others will be presented in T. S. Tanaka et al. (2025, in preparation).

With a nonevolving mass relation, our analysis supports the prediction of J. Li et al. (2025b) for the existence of a large population of lower-mass black holes to be discovered with deeper spectroscopy or different observing strategies. J. Li et al. (2025a) find lower-mass black holes, consistent with the local mass relation, in a search of the JWST archive of high-z massive galaxies with NIRSpec spectroscopy. S. Geris et al. (2026) further identified a population of low-mass black holes located within the scatter of the local relation. Also, W. Ren et al. (2025) identify candidates below the local relation based on NIRSpec IFU observations of typical star-forming galaxies from the ALPINE-CRISTAL survey. These are likely just the start in expanding the parameter space in black hole and galaxy mass for larger samples of SMBHs with JWST, which will allow the slope to be measured directly, thus placing tighter constraints on the normalization and intrinsic scatter of the mass relation.

Acknowledgments

J.S. led the writing of the paper and co-led the SHELLQs–JWST program. J.L. is responsible for the modeling analysis, preparation of figures, and contributions to the text. Measurements of stellar mass based on image decomposition was carried out by X.D., while black hole masses were determined by M.O. The remainder of the team participated in the interpretation of the results and review of the manuscript. We thank the anonymous referee for the insightful review and Jenny Greene for input on the local dispersion in the mass relation.

This work is based on observations made with the NASA/ESA/CSA James Webb Space Telescope. The data were obtained from the Mikulski Archive for Space Telescopes at the Space Telescope Science Institute, which is operated by the Association of Universities for Research in Astronomy, Inc., under NASA contract NAS 5-03127 for JWST. These

observations are associated with programs GO #1967 and GO #3859. The specific observations analyzed can be accessed via DOI: 10.17909/719q-cn32. Support for these programs was provided by NASA through a grant from the Space Telescope Science Institute, which is operated by the Association of Universities for Research in Astronomy, Inc., under NASA contract NAS 5-03127. This work was supported by World Premier International Research Center Initiative (WPI), MEXT, Japan. This work used computing resources at Kavli IPMU. J.S. is supported by JSPS KAKENHI (JP22H01262). M.O. is supported by the Japan Society for the Promotion of Science (JSPS) KAKENHI grant No. 24K22894. Y.M. was supported by the Japan Society for the Promotion of Science (JSPS) KAKENHI grant No. 21H04494. M.V. gratefully acknowledges financial support from the Independent Research Fund Denmark via grant numbers DFF 8021-00130 and 3103-00146 and from the Carlsberg Foundation via grant CF23-0417. S.E.I.B. is supported by the Deutsche Forschungsgemeinschaft (DFG) under Emmy Noether grant number BO 5771/1-1. K.I. acknowledges support from the National Natural Science Foundation of China (12073003, 11721303, 11991052). K.I. acknowledges support under the grant PID2022-136827NB-C44 provided by MCIN/AEI/10.13039/501100011033 / FEDER, UE. A.L. acknowledges support from PRIN MUR 2022— Project "2022935STW." J.T.S. is supported by the Deutsche Forschungsgemeinschaft (DFG, German Research Foundation)—project number 518006966. F.W. acknowledges support from NSF award AST-2513040. M.H. acknowledges support from the FNS under the SNSF starting grant 218032. B.T. acknowledges support from the European Research Council (ERC) under the European Union's Horizon 2020 research and innovation program (grant agreement number 950533) and from the Excellence Cluster ORIGINS, which is funded by the Deutsche Forschungsgemeinschaft (DFG, German Research Foundation) under Germany's Excellence Strategy—EXC 2094—390783311.

ORCID iDs

John David Silverman https://orcid.org/0000-0002-0000-6977
Junyao Li https://orcid.org/0000-0002-1605-915X
Xuheng Ding https://orcid.org/0000-0001-8917-2148
Masafusa Onoue https://orcid.org/0000-0003-2984-6803
Michael A. Strauss https://orcid.org/0000-0002-0106-7755
Yoshiki Matsuoka https://orcid.org/0000-0001-5063-0340
Takuma Izumi https://orcid.org/0000-0001-9452-0813
Knud Jahnke https://orcid.org/0000-0003-3804-2137
Tommaso Treu https://orcid.org/0000-0002-8460-0390
Marta Volonteri https://orcid.org/0000-0002-3216-1322
Camryn L. Phillips https://orcid.org/0000-0002-2099-0254
Irham T. Andika https://orcid.org/0000-0001-6102-9526
Kentaro Aoki https://orcid.org/0000-0003-4569-1098
Junya Arita https://orcid.org/0009-0007-0864-7094
Shunsuke Baba https://orcid.org/0000-0002-9850-6290
Sarah E. I. Bosman https://orcid.org/0000-0001-8582-7012
Anna-Christina Eilers https://orcid.org/0000-0003-2895-6218
Seiji Fujimoto https://orcid.org/0000-0001-7201-5066
Zoltan Haiman https://orcid.org/0000-0003-3633-5403
Masatoshi Imanishi https://orcid.org/0000-0001-6186-8792
Kohei Inayoshi https://orcid.org/0000-0001-9840-4959
Kazushi Iwasawa https://orcid.org/0000-0002-4923-3281
Nobunari Kashikawa https://orcid.org/0000-0003-3954-4219
Toshihiro Kawaguchi https://orcid.org/0000-0002-3866-9645
Chien-Hsiu Lee https://orcid.org/0000-0003-1700-5740
Alessandro Lupi https://orcid.org/0000-0001-6106-7821
Tohru Nagao https://orcid.org/0000-0002-7402-5441
Jan-Torge Schindler https://orcid.org/0000-0002-4544-8242
Malte Schramm https://orcid.org/0000-0001-7825-0075
Kazuhiro Shimasaku https://orcid.org/0000-0002-2597-2231
Yoshiki Toba https://orcid.org/0000-0002-3531-7863
Benny Trakhtenbrot https://orcid.org/0000-0002-3683-7297
Hideki Umehata https://orcid.org/0000-0003-1937-0573
Marianne Vestergaard https://orcid.org/0000-0001-9191-9837
Fabian Walter https://orcid.org/0000-0003-4793-7880
Feige Wang https://orcid.org/0000-0002-7633-431X
Jinyi Yang https://orcid.org/0000-0001-5287-4242

References

Aihara, H., Arimoto, N., Armstrong, R., et al. 2018, PASJ, 70, S4
Arita, J., Kashikawa, N., Matsuoka, Y., et al. 2023, ApJ, 954, 210
Bennert, V. N., Treu, T., Ding, X., et al. 2021, ApJ, 921, 36
Bentz, M. C., & Manne-Nicholas, E. 2018, ApJ, 864, 146
Chabrier, G. 2003, PASP, 115, 763
Cisternas, M., Jahnke, K., Bongiorno, A., et al. 2011, ApJL, 741, L11
Dattathri, S., Natarajan, P., Porras-Valverde, A. J., et al. 2025, ApJ, 984, 122
Decarli, R., Dotti, M., Bañados, E., et al. 2019, ApJ, 880, 157
Ding, X., Birrer, S., Treu, T., & Silverman, J. D. 2021, arXiv:2111.08721
Ding, X., Onoue, M., Silverman, J. D., et al. 2023, Natur, 621, 51
Ding, X., Onoue, M., Silverman, J. D., et al. 2025, ApJ, 993, 91
Ding, X., Silverman, J., Treu, T., et al. 2020a, ApJ, 888, 37
Ding, X., Silverman, J. D., & Onoue, M. 2022a, ApJL, 939, L28
Ding, X., Silverman, J. D., Treu, T., et al. 2022b, ApJ, 933, 132
Ding, X., Treu, T., Silverman, J. D., et al. 2020b, ApJ, 896, 159
Eilers, A.-C., Mackenzie, R., Pizzati, E., et al. 2024, ApJ, 974, 275
Foreman-Mackey, D., Hogg, D. W., Lang, D., & Goodman, J. 2013, PASP, 125, 306
Geris, S., Maiolino, R., Isobe, Y., et al. 2026, MNRAS, 545, staf1979
Greene, J. E., Labbe, I., Goulding, A. D., et al. 2024, ApJ, 964, 39
Greene, J. E., Strader, J., & Ho, L. C. 2020, ARA&A, 58, 257
Gültekin, K., Richstone, D. O., Gebhardt, K., et al. 2009, ApJ, 698, 198
Habouzit, M., Li, Y., Somerville, R. S., et al. 2021, MNRAS, 503, 1940
Habouzit, M., Onoue, M., Bañados, E., et al. 2022, MNRAS, 511, 3751
Harikane, Y., Zhang, Y., Nakajima, K., et al. 2023, ApJ, 959, 39
Inayoshi, K., Visbal, E., & Haiman, Z. 2020, ARA&A, 58, 27
Izumi, T., Onoue, M., Matsuoka, Y., et al. 2019, PASJ, 71, 111
Jahnke, K., & Macciò, A. V. 2011, ApJ, 734, 92
Jahnke, K., Sánchez, S. F., Wisotzki, L., et al. 2004, ApJ, 614, 568
Jones, B. L., Kocevski, D. D., Pacucci, F., et al. 2025, arXiv:2510.07376
Kocevski, D. D., Finkelstein, S. L., Barro, G., et al. 2025, ApJ, 986, 126
Kormendy, J., & Ho, L. C. 2013, ARA&A, 51, 511
Lauer, T. R., Tremaine, S., Richstone, D., & Faber, S. M. 2007, ApJ, 670, 249
Li, J., Shen, Y., & Zhuang, M.-Y. 2025a, arXiv:2502.05048
Li, J., Silverman, J. D., Ding, X., et al. 2021, ApJ, 922, 142
Li, J., Silverman, J. D., Izumi, T., et al. 2022, ApJL, 931, L11
Li, J., Silverman, J. D., Shen, Y., et al. 2025b, ApJ, 981, 19
Li, R., Ho, L. C., & Chen, C.-H. 2025c, arXiv:2505.12867
Lupi, A., Trinca, A., Volonteri, M., Dotti, M., & Mazzucchelli, C. 2024, A&A, 689, A128
Maiolino, R., Scholtz, J., Curtis-Lake, E., et al. 2024a, A&A, 691, A145
Maiolino, R., Scholtz, J., Witstok, J., et al. 2024b, Natur, 627, 59
Marques-Chaves, R., Schaerer, D., Dessauges-Zavadsky, M., et al. 2025, arXiv:2510.12411
Marshall, M. A., Yue, M., Eilers, A.-C., et al. 2025, A&A, 702, A50
Matsuoka, Y., Iwasawa, K., Onoue, M., et al. 2018a, ApJS, 237, 5

Matsuoka, Y., Iwasawa, K., Onoue, M., et al. 2022, ApJS, 259, 18
Matsuoka, Y., Onoue, M., Kashikawa, N., et al. 2016, ApJ, 828, 26
Matsuoka, Y., Onoue, M., Kashikawa, N., et al. 2018b, PASJ, 70, S35
Matsuoka, Y., Onoue, M., Iwasawa, K., et al. 2025, ApJ, 988, 57
Matsuoka, Y., Strauss, M. A., Kashikawa, N., et al. 2018c, ApJ, 869, 150
Matthee, J., Naidu, R. P., Brammer, G., et al. 2024, ApJ, 963, 129
Mechtley, M., Jahnke, K., Windhorst, R. A., et al. 2016, ApJ, 830, 156
Miyazaki, S., Komiyama, Y., Kawanomoto, S., et al. 2018, PASJ, 70, S1
Morishita, T., Abramson, L. E., Treu, T., et al. 2019, ApJ, 877, 141
Ni, Y., Di Matteo, T., Bird, S., et al. 2022, MNRAS, 513, 670
Onoue, M., Ding, X., Silverman, J. D., et al. 2025, NatAs, 9, 1541
Onoue, M., Inayoshi, K., Ding, X., et al. 2023, ApJL, 942, L17
Pacucci, F., Nguyen, B., Carniani, S., Maiolino, R., & Fan, X. 2023, ApJL, 957, L3
Peng, C. Y., Impey, C. D., Rix, H.-W., et al. 2006, ApJ, 649, 616
Pillepich, A., Springel, V., Nelson, D., et al. 2018, MNRAS, 473, 4077
Reines, A. E., & Volonteri, M. 2015, ApJ, 813, 82
Ren, W., Silverman, J. D., Fassist, A. L., et al. 2025, MNRAS, 544, 211
Richards, G. T., Lacy, M., Storrie-Lombardi, L. J., et al. 2006, ApJS, 166, 470
Rigby, J., Perrin, M., McElwain, M., et al. 2023, PASP, 135, 048001
Schaye, J., Crain, R. A., Bower, R. G., et al. 2015, MNRAS, 446, 521
Schulze, A., & Wisotzki, L. 2011, A&A, 535, A87
Schulze, A., & Wisotzki, L. 2014, MNRAS, 438, 3422
Shen, Y., Greene, J. E., Ho, L. C., et al. 2015, ApJ, 805, 96
Shen, Y., Grier, C. J., Horne, K., et al. 2024, ApJS, 272, 26
Shuntov, M., Ilbert, O., Toft, S., et al. 2025, A&A, 695, A20
Stevens, A. R. H., Croton, D. J., & Mutch, S. J. 2016, MNRAS, 461, 859
Stevens, A. R. H., Lagos, C. d. P., Obreschkow, D., & Sinha, M. 2018, MNRAS, 481, 5543
Stone, M. A., Lyu, J., Rieke, G. H., & Alberts, S. 2023, ApJ, 953, 180
Stone, M. A., Lyu, J., Rieke, G. H., Alberts, S., & Hainline, K. N. 2024, ApJ, 964, 90
Sun, M., Trump, J. R., Brandt, W. N., et al. 2015, ApJ, 802, 14
Sun, Y., Rieke, G. H., Lyu, J., et al. 2025b, ApJ, 983, 165
Sun, Y., Rieke, G. H., Lyu, J., et al. 2025a, ApJ, 983, 165
Tanaka, T. S., Silverman, J. D., Ding, X., et al. 2025, ApJ, 979, 215
Treu, T., Woo, J.-H., Malkan, M. A., & Blandford, R. D. 2007, ApJ, 667, 117
Vestergaard, M., & Peterson, B. M. 2006, ApJ, 641, 689
Volonteri, M., Dubois, Y., Pichon, C., & Devriendt, J. 2016, MNRAS, 460, 2979
Volonteri, M., Habouzit, M., & Colpi, M. 2021, NatRP, 3, 732
Wang, F., Yang, J., Fan, X., et al. 2024, ApJ, 968, 9
Wu, J., Shen, Y., Jiang, L., et al. 2022, MNRAS, 517, 2659
Yue, M., Eilers, A.-C., Simcoe, R. A., et al. 2024, ApJ, 966, 176